



Modeling Phase-Locked Loop-Based Synchronization in Grid-Interfaced Converters

Zhi-Xiang Zou , Member, IEEE, and Marco Liserre , Fellow, IEEE

Abstract—Grid converters need a synchronization which is often a phase-locked loop (PLL) to get connected to the grid. In the literature, impedance-based models using small-signal technique have been widely utilized to describe the behaviors of PLL-synchronized grid converter. However, most of them target at specific problems and are able to represent the phenomenon under certain scenarios. For the analysis during phase transient, like phase jump due to grid fault, an accurate model is still missing. To address this issue, a general impedance-based model using Maclaurin expansions for its trigonometric function approximation has been proposed in this paper, so that it can well represent the system behavior during phase transient. Moreover, different deepness of the general model can be scaled, leading to different models including phasorial model, current source model, impedance-based model with/without PLL effects. A guideline on how to choose a proper model based on the problems to be studied and grid conditions has been provided in this paper. Simulation and experimental results are given to validate the effectiveness of the model and the theoretical analysis.

Index Terms—Grid converter, synchronization, phase-locked loop (PLL), Maclaurin expansions, model accuracy, model deepness, stability analysis.

I. INTRODUCTION

A FUNDAMENTAL change of paradigm has been proposed in the context of power systems, namely increasing utilization of power electronics interfaces, for instance, grid-interfaced power converters. Due to lack of inertia, grid converters do not inherently preserve the phase shift and phase sequencing during grid-connected operation. Commonly, a phase-locked loop (PLL) is adopted by grid converters for grid synchronization [1], [2]. When the penetration level of grid converters is low, the influence of PLL behavior is negligible comparing to the inertia response of other power system components. However, in modern power systems, especially inertia-less grids which are dominated by power converters, ignoring the effects of synchronization will lead to misjudge the grid characteristics and stability [3]–[5].

Manuscript received April 5, 2019; revised July 26, 2019; accepted August 26, 2019. Date of publication September 4, 2019; date of current version February 19, 2020. This work was supported by the German Research Foundation [LI 1878/4-1] - Formal stability assessment of hybrid distribution grids based on the correct modeling of the effect of synchronization of the power electronics interfaces. Paper no. TEC-00370-2019. (Corresponding author: Zhi-Xiang Zou.)

Z.-X. Zou is with the School of Electrical Engineering, Southeast University, Nanjing 210096, China (e-mail: zz@tf.uni-kiel.de).

M. Liserre is with the Chair of Power Electronics, Christian-Albrechts Universität zu Kiel, Kiel 24143, Germany (e-mail: ml@tf.uni-kiel.de).

Color versions of one or more of the figures in this article are available online at <http://ieeexplore.ieee.org>.

Digital Object Identifier 10.1109/TEC.2019.2939425

To well study the characteristics of a power converter-dominated grid, the key challenge is to develop an accurate model of grid converters with the consideration of synchronization, meanwhile keeping computational effort in a reasonable level. One popular methodology to cope with modeling of grid converter as well as synchronization is to use impedance-based model, which is derived from the small-signal modeling techniques [6], [7]. Impedance-based models considering the PLL effects have been developed in both synchronous frame and stationary frame [8]–[10]. However, the motivations of the developed models are usually to study specific problems, for instance, the impedance-based model with PLL in the literature is to study the static stability issue, assuming the voltage at the interconnection point is stiff and the phase deviation between grid and PLL is insignificant. Coming to an actual grid, there are different problem formulations and grid conditions, each conventional model may have its limitation. Taking the phase transient as an example, the conventional impedance-based model considering PLL effects can hardly represent the system behaviors and thus it could lead to incorrect stability assessment.

To bridge this gap, this paper attempts to expand the conventional impedance-based model to a general way in order to study different problems under different grid representation scenarios, especially the stability issues during phase transient. A guideline to model PLL-synchronized grid converter is proposed in this paper based on the problems and grid conditions. Instead of the most accurate model, the most efficient model is offered for each scenario by considering both complexity and accuracy under the circumstance. The rest of the paper is organized as follows: The small-signal model of the PLL-based grid synchronization is presented in Section II, the full model of the PLL-synchronized grid converter is developed in Section III, the model deepness and accuracy of different models based on the developed full model are discussed in Section IV, the model guideline is illustrated in this section, simulation and experimental results are provided in Section V to validate the theoretical analysis, Section VI draws the conclusions.

II. SMALL-SIGNAL MODEL OF GRID SYNCHRONIZATION

The most extended grid synchronization technique used in three-phase power converters is the PLL based on the synchronous reference frame (SRF-PLL) [11]. The schematic diagram of a SRF-PLL is presented in Fig. 1, where the three-phase voltage vector $[v_a, v_b, v_c]^T$ is translated from *abc*-frame

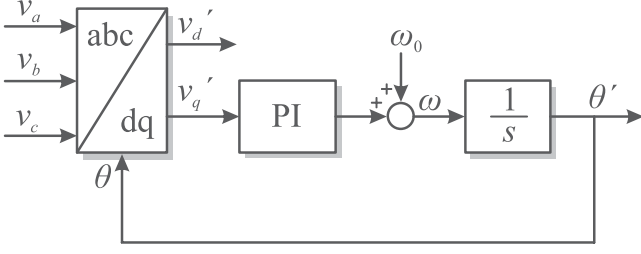


Fig. 1. Schematic diagram of a synchronous reference frame PLL.

to dq -frame by the Park's transformation, the phase angle θ' is regulated by a PI controller. The control objective is to regulate the q -component to zero, once v_q' is zero, the PLL is well locked. Under this circumstance, the phase displacement between the actual phase and the detected phase is zero during the steady state.

The Park transform of the SRF-PLL holds nonlinearity. A linearization procedure is required, where the transform matrix can be split up into two parts:

$$\mathbf{T}(\theta') = \sqrt{\frac{2}{3}} \begin{bmatrix} \cos(\theta') & \cos(\theta' - \frac{2\pi}{3}) & \cos(\theta' + \frac{2\pi}{3}) \\ -\sin(\theta') & -\sin(\theta' - \frac{2\pi}{3}) & -\sin(\theta' + \frac{2\pi}{3}) \end{bmatrix} \\ = \begin{bmatrix} \cos(\Delta\theta') & \sin(\Delta\theta') \\ -\sin(\Delta\theta') & \cos(\Delta\theta') \end{bmatrix} \cdot \mathbf{T}(\theta_0) \quad (1)$$

where $\Delta\theta' = \theta' - \theta_0$ indicates the phase displacement between the actual phase θ_0 and the detected phase θ' . In the literature, it is seen that the double-frequency terms have been considered in the transform matrix for the single-phase power-based PLL, due to the product-to-sum trigonometric identity [12]. Moreover, the double-frequency terms could emerge in the coordinate frame of a three-phase PLL under unbalanced grid condition [13], because of the effects of negative-sequence component. Since this work mainly focuses the modeling issues of converter in a symmetric three-phase grid, the double-frequency terms would not appear in the system and thereby will not be considered in the following procedures for the sake of analysis convenience.

During steady state, assuming the PI controller is well tuned, $\Delta\theta' \approx 0$. Thus, $\cos(\Delta\theta') \approx 1$ and $\sin(\Delta\theta') \approx \Delta\theta'$ are valid, and (1) becomes

$$\mathbf{T}(\theta') \approx \begin{bmatrix} 1 & \Delta\theta' \\ -\Delta\theta' & 1 \end{bmatrix} \cdot \mathbf{T}(\theta_0) \quad (2)$$

By applying the transform, the d and q components of the grid voltage v_d' and v_q' seen by the PLL can be obtained by

$$\begin{bmatrix} v_d' \\ v_q' \end{bmatrix} \approx \begin{bmatrix} 1 & \Delta\theta' \\ -\Delta\theta' & 1 \end{bmatrix} \begin{bmatrix} v_d \\ v_q \end{bmatrix} \quad (3)$$

where v_d and v_q are the actual d and q components of the grid voltage, i.e., by applying $\mathbf{T}(\theta_0)$. For better understanding, the phasor diagram of the PLL-synchronized grid converter is illustrated in Fig. 2, where two synchronous frames are considered: the frame of the actual grid voltage (d_{grid}/q_{grid}), and

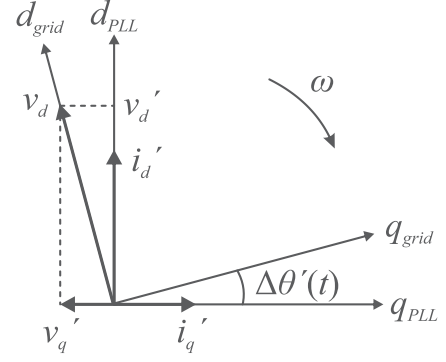


Fig. 2. Phasor diagram of PLL-synchronized grid converter.

the frame of the PLL (d_{PLL}/q_{PLL}). v_d and v_q are aligned with d_{grid}/q_{grid} , while v_d' and v_q' are aligned with d_{PLL}/q_{PLL} pursuing towards d_{grid}/q_{grid} . If the control bandwidth of the grid converter is high enough, the converter current is aligned with the grid voltage seen by the PLL.

Assuming the actual grid voltages in dq -frame are $v_d = V_d + \Delta v_d$ and $v_q = V_q + \Delta v_q$, here V_d , V_q and Δv_d , Δv_q are the dc quantities and the small-signal perturbations of the grid voltage in dq -frame, the small-signal equations of (3) can be rewritten by

$$\begin{bmatrix} \Delta v_d' \\ \Delta v_q' \end{bmatrix} = \begin{bmatrix} \Delta v_d \\ \Delta v_q \end{bmatrix} + \begin{bmatrix} V_q \\ -V_d \end{bmatrix} \Delta\theta' \quad (4)$$

where $\Delta v_d'$ and $\Delta v_q'$ are the small-signal perturbations of the voltage seen by the PLL.

According to the schematic shown in Fig. 1, the open-loop error transfer function is

$$H_e(s) = \frac{\Theta'(s)}{V_q'(s)} = G_{PI}(s)G_{VCO}(s) = \frac{k_{ppll}s + k_{ipll}}{s^2} \quad (5)$$

where $G_{PI}(s)$ and $G_{VCO}(s)$ are the transfer functions of the PI controller and the voltage-controlled oscillator (VCO), respectively. Combining (4) and (5) in frequency domain, one can obtain:

$$\begin{bmatrix} \Delta v_d' \\ \Delta v_q' \end{bmatrix} = \begin{bmatrix} 1 & V_q G_{PLL}(s) \\ 0 & 1 - V_d G_{PLL}(s) \end{bmatrix} \begin{bmatrix} \Delta v_d \\ \Delta v_q \end{bmatrix} \quad (6)$$

where $G_{PLL}(s)$ is the open-loop phase transfer function, and its expression is given by

$$G_{PLL}(s) = \frac{\Theta'(s)}{V_q(s)} = \frac{H_e(s)}{1 + V_d H_e(s)} \quad (7)$$

III. MODEL OF PLL-SYNCHRONIZED CONVERTER

It is worth noting that the conventional small-signal model of grid synchronization relied on the assumption $\Delta\theta \approx 0$. In this regard, the first-order approximation of the trigonometric functions is used in (2). The model developed in Section II can well describe the system behaviors during steady state or the phase perturbation is very small. Based on the small-angle approximation [14], the first-order approximation can remain

accuracy when $\Delta\theta \leq 7^\circ$. However, in an actual grid, larger phase perturbation could happen, for instance, during grid faults. The grid codes in Northern Europe require renewable energy systems to withstand sudden phase jumps up to $\pm 30^\circ$ and frequency variation between 47.5 Hz–51.5 Hz [15], [16]. The first-order approximation is no longer accurate for the large phase jump case study. To overcome the issue, the full Maclaurin expansions of the trigonometric functions are used in the angle approximation, which are

$$\sin(\Delta\theta') = \sum_{n=0}^{\infty} \frac{(-1)^n}{(2n+1)!} (\Delta\theta')^{2n+1} \quad (8)$$

$$\cos(\Delta\theta') = \sum_{n=0}^{\infty} \frac{(-1)^n}{(2n)!} (\Delta\theta')^{2n} \quad (9)$$

A. Higher-Order Model of Grid Synchronization

Using the full Maclaurin expansions, (3) can be updated to adapt to large phase perturbation:

$$\begin{bmatrix} v_d' \\ v_q' \end{bmatrix} = \begin{bmatrix} \sum_{n=0}^{\infty} \frac{(-1)^n}{(2n)!} (\Delta\theta')^{2n} & \sum_{n=0}^{\infty} \frac{(-1)^n}{(2n+1)!} (\Delta\theta')^{2n+1} \\ -\sum_{n=0}^{\infty} \frac{(-1)^n}{(2n+1)!} (\Delta\theta')^{2n+1} & \sum_{n=0}^{\infty} \frac{(-1)^n}{(2n)!} (\Delta\theta')^{2n} \end{bmatrix} \cdot \begin{bmatrix} v_d \\ v_q \end{bmatrix} \quad (10)$$

Then, the small-signal equation of (10) can be written by

$$\begin{bmatrix} \Delta v_d' \\ \Delta v_q' \end{bmatrix} = \begin{bmatrix} \Delta v_d \\ \Delta v_q \end{bmatrix} + \begin{bmatrix} V_q \\ -V_d \end{bmatrix} \Delta\theta' + \frac{1}{2!} \begin{bmatrix} -V_d \\ -V_q \end{bmatrix} \Delta\theta'^2 + \dots \quad (11)$$

When applying the transform to the converter current, the small-signal equation of the converter current can be derived by a similar way:

$$\begin{bmatrix} \Delta i_d' \\ \Delta i_q' \end{bmatrix} = \begin{bmatrix} \Delta i_d \\ \Delta i_q \end{bmatrix} + \begin{bmatrix} I_q \\ -I_d \end{bmatrix} \Delta\theta' + \frac{1}{2!} \begin{bmatrix} -I_d \\ -I_q \end{bmatrix} \Delta\theta'^2 + \dots \quad (12)$$

where $\Delta i_d'$ and $\Delta i_q'$ are the small-signal perturbations of the converter current in dq -frame aligning with the PLL frame, Δi_d and Δi_q are the small-signal perturbations of the actual converter current, I_d and I_q are the amplitudes of d and q components of the converter current.

B. Full Model of PLL-Synchronized Converter

In the literature, current-controlled and power-controlled schemes are utilized, and both of them essentially regulate the three-phase converter current $[i_a, i_b, i_c]^T$ [11]. Moreover, the PCC voltage amplitude is assumed to be constant in this paper for the convenience so that the effects of the power loop shown in Fig. 3 can be ignored. The current-controlled scheme with

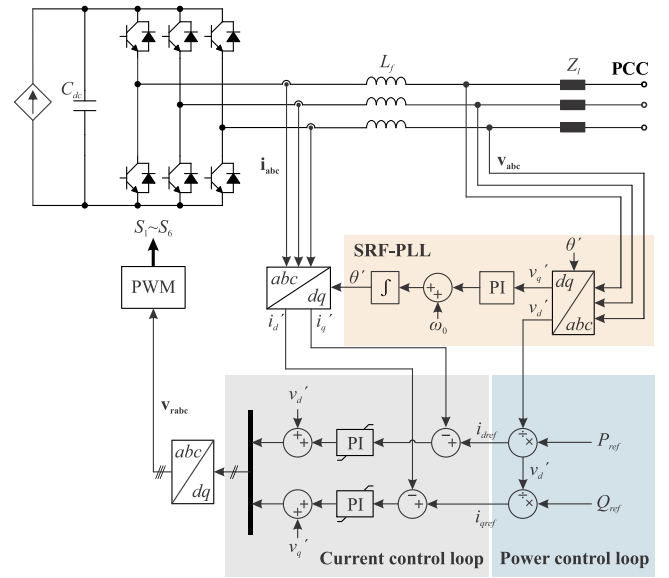


Fig. 3. System configuration of a grid-interfaced converter.

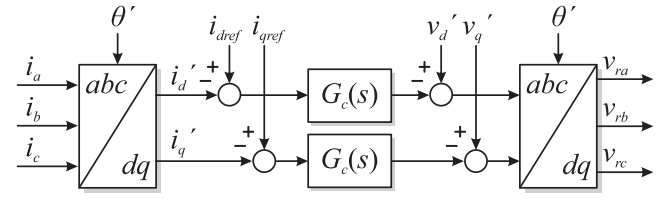


Fig. 4. System configuration of a grid-interfaced converter.

single current loop in the synchronous frame is considered in the modeling of this paper and is shown in Fig. 4. Given the three-phase voltage of PCC $[v_a, v_b, v_c]^T$, the average model of the grid converter in abc frame is

$$L_f \frac{d}{dt} \begin{bmatrix} i_a \\ i_b \\ i_c \end{bmatrix} = G_d \begin{bmatrix} v_{ra} \\ v_{rb} \\ v_{rc} \end{bmatrix} - \begin{bmatrix} v_a \\ v_b \\ v_c \end{bmatrix} \quad (13)$$

where L_f is the inductance of output filter, $[v_{ra}, v_{rb}, v_{rc}]^T$ are the reference voltage of the grid converter, and G_d represents the computation and PWM delay. Using an ideal transform, the average model in dq frame is obtained by

$$\begin{bmatrix} L_f s & -\omega L_f \\ \omega L_f & L_f s \end{bmatrix} \begin{bmatrix} i_d \\ i_q \end{bmatrix} = \begin{bmatrix} G_d & 0 \\ 0 & G_d \end{bmatrix} \begin{bmatrix} v_{rd} \\ v_{rq} \end{bmatrix} - \begin{bmatrix} v_d \\ v_q \end{bmatrix} \quad (14)$$

It is worth noting that the d and q components in (4) are obtained by applying ideal transform $\mathbf{T}(\theta_0)$, namely both components are directly oriented with the actual PCC voltage \mathbf{v}_{abc} , and thus they do not rely on the PLL characteristics. On the other hand, the d and q components in the current control system do rely on the PLL. According to the control scheme in Fig. 4, the perturbation equation of current control is

$$\begin{bmatrix} \Delta v_{rd}' \\ \Delta v_{rq}' \end{bmatrix} = \begin{bmatrix} G_c & 0 \\ 0 & G_c \end{bmatrix} \begin{bmatrix} \Delta i_{dref} - \Delta i_d' \\ \Delta i_{qref} - \Delta i_q' \end{bmatrix} + \begin{bmatrix} \Delta v_d' \\ \Delta v_q' \end{bmatrix} \quad (15)$$

where $[\Delta i_{dref}, \Delta i_{qref}]^T$ are the current reference perturbations in dq frame, $[\Delta v'_{rd}, \Delta v'_{rq}]^T$ are the reference voltage perturbations in dq frame, and G_c represents the current controller. Noting that, all the d and q components in (15) are obtained by applying the transform with PLL phase angle, which is $T(\theta')$. As a result, the corresponding variables in (15) are with the superscript $(\cdot)'$, indicating the influences of PLL are considered.

To decouple the PLL effects, the linearization procedures previously mentioned can be applied to the variables which correspond to the (inverse) transform. The small-signal expressions for the voltage and current transform are given by (11) and (12), respectively. For the reference voltage inverse transform, i.e., $[\Delta v'_{rd}, \Delta v'_{rq}]^T$, the expression can be illustrated as

$$\begin{bmatrix} \Delta v_{rd} \\ \Delta v_{rq} \end{bmatrix} = \begin{bmatrix} \Delta v'_{rd} \\ \Delta v'_{rq} \end{bmatrix} + \begin{bmatrix} -V'_{rq} \\ V'_{rd} \end{bmatrix} \Delta\theta' + \frac{1}{2!} \begin{bmatrix} V'_{rd} \\ V'_{rq} \end{bmatrix} \Delta\theta'^2 + \dots \quad (16)$$

where V'_{rd} and V'_{rq} are the amplitudes of the reference voltage in dq frame.

By substituting (11), (12), and (16) into (14), one can get the complete model of the grid converter with the PLL effects:

$$\begin{bmatrix} \Delta i_d \\ \Delta i_q \end{bmatrix} = \mathbf{I}_{eq} \begin{bmatrix} \Delta i_{dref} \\ \Delta i_{qref} \end{bmatrix} + \mathbf{Y}_{eq} \begin{bmatrix} \Delta v_d \\ \Delta v_q \end{bmatrix} + \begin{bmatrix} \Theta_{d1} \\ \Theta_{q1} \end{bmatrix} \Delta\theta' + \begin{bmatrix} \Theta_{d2} \\ \Theta_{q2} \end{bmatrix} (\Delta\theta')^2 + \dots \quad (17)$$

where

$$\mathbf{I}_{eq} = \begin{bmatrix} I_{dd} & I_{dq} \\ I_{qd} & I_{qq} \end{bmatrix}; \mathbf{Y}_{eq} = \begin{bmatrix} I_{dd} & I_{dq} \\ I_{qd} & I_{qq} \end{bmatrix} \quad (18)$$

All the detailed expressions of the matrix elements in (17) and (18) are given in the Appendix.

IV. MODEL DEEPNESS AND ACCURACY EVALUATION

This section starts with the explanation of the model representations of (17). Phasorial model, current source model, impedance-based model without/with the effects of PLL, and impedance-based model for phase transient are discussed and evaluated in terms of accuracy in this section.

From the model of (17), it can be seen that four sets of terms are included. Each of them can represent the grid converter with certain model deepness as well as model accuracy. It is important noting that an imperfect model with lower deepness could lead to under/overestimation of the system response to certain phenomena, while a perfect model with higher deepness usually requires higher computation efforts during analysis or simulation, which can be limited by the real-time simulation capability. In this context, a guideline in modeling the grid converter for power system as well as power electronics is presented in this paper. Four different types of models with different modeling deepness are illustrated in the following. The model accuracy, scope of study, and limitation of each model are discussed in detail.

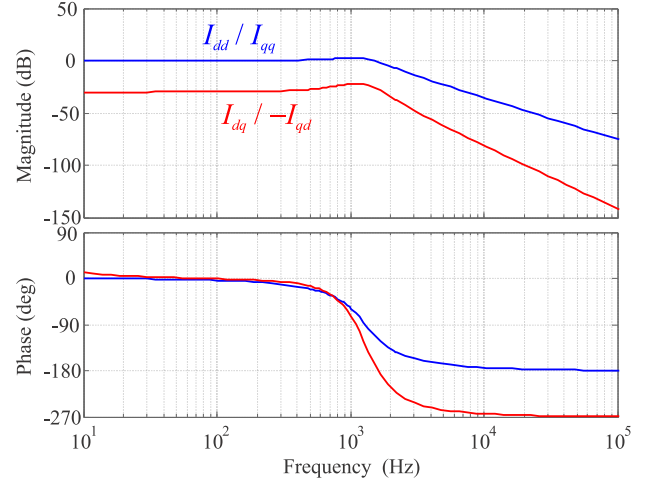


Fig. 5. Bode diagrams of equivalent current sources of grid converter: blue - diagonal elements of current source matrix (I_{dd} , I_{qq}), red - non-diagonal elements of current source matrix (I_{dq} , I_{qd}).

TABLE I
SYSTEM PARAMETERS

Symbol	Quantity	Value
L_f	Output filter of grid inverter	5 mH
T_s	sampling frequency	10 kHz
k_{pc}	proportional gain of current control	15
k_{ic}	integral gain of current control	250
k_{ppll}	proportional gain of PLL	18.4
k_{ipll}	integral gain of PLL	169.3

A. Current Source Model and Phasorial Model

The simplest representation obtained from (17) is the current source model, which is

$$\begin{bmatrix} \Delta i_d \\ \Delta i_q \end{bmatrix} = \mathbf{I}_{eq} \begin{bmatrix} \Delta i_{dref} \\ \Delta i_{qref} \end{bmatrix} \quad (19)$$

The current source matrix of \mathbf{I}_{eq} is given in (18) and the detailed expressions in the Appendix. The matrix of \mathbf{I}_{eq} represents the nature of the current control, which is essentially the closed-loop transfer function matrix of the current control system. The Bode diagram of the diagonal elements of \mathbf{I}_{eq} : I_{dd} and I_{qq} , and the non-diagonal elements: I_{dq} and I_{qd} are shown in Fig. 5 by the blue and the red curves, respectively. The magnitudes of the non-diagonal elements are much lower than those of the diagonal elements, thus the control coupling effects can be usually ignored during linear analysis. The control performance of the grid converter, in terms of steady-state and dynamic performance, can be directly interpreted by the characteristics of I_{dd} and I_{qq} .

The control parameters in Table I are used for the Bode diagram study. The proportional and integral gains of the current control are designed to achieve a sufficient phase margin (i.e., 70.7°) and meanwhile a high system bandwidth, which is

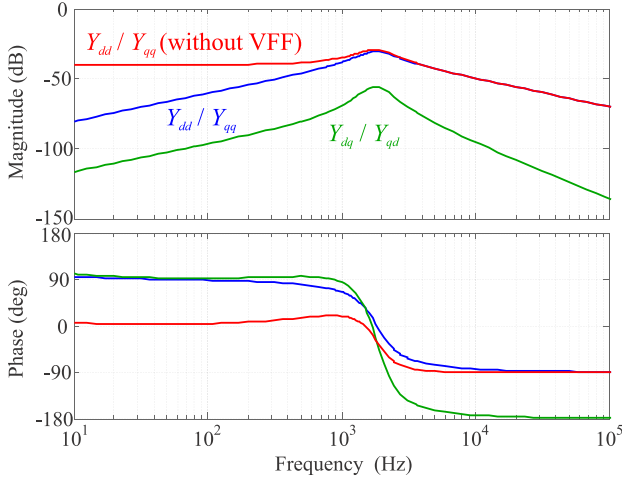


Fig. 6. Bode diagrams of equivalent admittances of grid converter: blue – self-admittance (Y_{dd} , Y_{qq}) using voltage feedforward (VFF), red – self-admittance without VFF, green – mutual-admittance (Y_{dq} , Y_{qd}).

1750 Hz as shown in the Bode diagram, so that the system can achieve zero steady-state error within the system bandwidth. The proportional and integral gains of the SRF-PLL are designed to achieve an optimal damped second-order system [17]. The detailed design procedure as well as formula for the SRF-PLL are given in the Appendix. The grid voltage disturbance could have very limited influence within the bandwidth, in particular at the fundamental frequency. In this regard, the current reference (for current-controlled scheme) or the power reference (for power-controlled scheme) can be directly used as the phasorial model for the power system analysis and optimization.

B. Impedance-Based Model Without PLL (0-Order)

In addition to equivalent current source, the grid voltage disturbance plays an important role on the system behaviors if its time constant can influence the responses in the study. With this consideration, the admittance-related term of (17) can be included, which is

$$\begin{bmatrix} \Delta i_d \\ \Delta i_q \end{bmatrix} = \mathbf{I}_{eq} \begin{bmatrix} \Delta i_{dref} \\ \Delta i_{qref} \end{bmatrix} + \mathbf{Y}_{eq} \begin{bmatrix} \Delta v_d \\ \Delta v_q \end{bmatrix} \quad (20)$$

Here, \mathbf{Y}_{eq} is the equivalent admittance matrix of the grid converter, which can represent the impacts of the grid voltage on the converter current. The Bode diagrams of the self-admittances, i.e., diagonal elements of \mathbf{Y}_{eq} : Y_{dd} and Y_{qq} , are shown in Fig. 6 by the blue curve, by using the system parameters listed in Table I. The mutual-admittances, i.e., non-diagonal elements of \mathbf{Y}_{eq} : Y_{dq} and Y_{qd} are presented in the same figure by the green curve. Since the magnitudes of these elements are much lower than those of the diagonal elements, indicating the effects of the non-diagonal elements are negligible.

The impacts of the voltage feedforward are studied and the Bode diagram of Y_{dd} and Y_{qq} without the voltage feedforward

are shown by the red curve in Fig. 6. Comparing to the self-admittance using the feedforward, it can be seen that the admittance profile in the low-frequency range (i.e., 10 Hz 1000 Hz) is modified, while the profile above the resonant frequency remains the same. This indicates that the voltage feedforward can contribute to the equivalent admittance within certain frequency range, but the admittance in the high-frequency range remains the same as it is usually dominated by the physical filter.

With the combination of \mathbf{I}_{eq} and \mathbf{Y}_{eq} , the model can better reveal the dynamic behaviors, especially the dynamics introduced by the grid voltage. Moreover, the impedance-based model is widely used in the harmonic stability analysis. Comparing to the eigenvalues analysis of the state matrix, impedance-based approach provides a more straightforward way and can be easily expanded to a multiple converters system as well as a balanced power system network [18], [19].

C. Impedance-Based Model With First-Order PLL Terms

As explain in the previous sections, the PLL is another important element of grid converter during stability analysis, especially when the grid converter being connected to a weak grid or the PLL bandwidth is high. Typically, the short-circuit ratio (SCR) can be used to define the stiffness of a grid, for instance, a grid with low SCR like $SCR < 3$ can be rearded as a weak grid [20].

If it is of interest the contribution of the PLL to the converter, the $\Delta\theta'$ -related terms have to be taken into account. For static analysis, since the first-order angle approximation is accurate enough for the trigonometric functions, the first-order terms of (17) can be included and the model is written by

$$\begin{aligned} \begin{bmatrix} \Delta i_d \\ \Delta i_q \end{bmatrix} &= \mathbf{I}_{eq} \begin{bmatrix} \Delta i_{dref} \\ \Delta i_{qref} \end{bmatrix} + \mathbf{Y}_{eq} \begin{bmatrix} \Delta v_d \\ \Delta v_q \end{bmatrix} + \begin{bmatrix} \Theta_{d1} \\ \Theta_{q1} \end{bmatrix} \Delta\theta' \\ &= \mathbf{I}_{eq} \begin{bmatrix} \Delta i_{dref} \\ \Delta i_{qref} \end{bmatrix} + \mathbf{Y}_{eq}^{\theta 1} \begin{bmatrix} \Delta v_d \\ \Delta v_q \end{bmatrix} \end{aligned} \quad (21)$$

$$Y_{dd}^{\theta 1} = Y_{dd}, Y_{qd}^{\theta 1} = Y_{qd},$$

$$Y_{dq}^{\theta 1} = Y_{dq} + \Theta_{d1} G_{PLL_op},$$

$$Y_{qq}^{\theta 1} = Y_{qq} + \Theta_{q1} G_{PLL_op}. \quad (22)$$

It can be seen that the first-order $\Delta\theta'$ -related terms contribute to the equivalent admittance matrix. Assuming the converter operates at unity power factor, it is expected to that the PLL effects on the d -axis of the equivalent admittance are negligible, while the q -axis of the equivalent admittance are modified when the PLL being taken into account. Comparisons of Bode diagrams of Y_{qq} and $Y_{qq}^{\theta 1}$ are presented in Fig. 7, where it can be seen that the magnitude as well as the phase of the q -axis self-admittance in the low-frequency range (i.e., 1 Hz 1000 Hz) have been significantly modified when considering the PLL effects. By tuning the PLL bandwidth (BW), it is observed that the profile of $Y_{qq}^{\theta 1}$ in the low-frequency range would be further changed.

From the point of view of harmonic stability, the system stability is determined by the ratio between grid impedance and

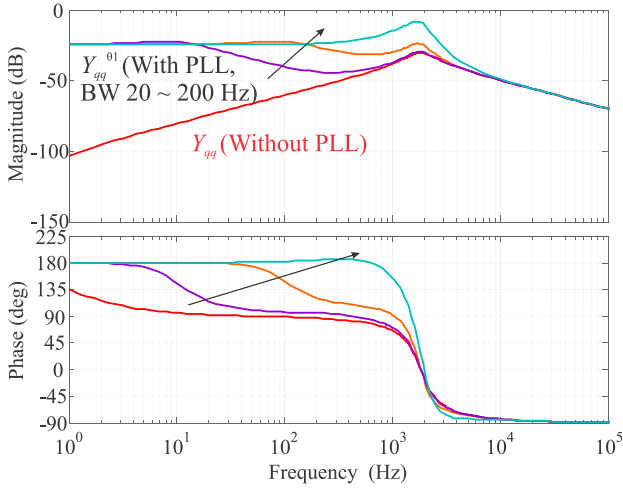


Fig. 7. Bode diagrams of equivalent admittances of grid converter with the consideration of PLL.

equivalent impedance of grid converter, which is $\mathbf{L} = \mathbf{Z}_g \cdot \mathbf{Y}_{qq}^{\theta 1}$, \mathbf{Z}_g is the grid impedance matrix. When the grid is strong, meaning the grid impedance is small, the interaction between \mathbf{Z}_g and $\mathbf{Y}_{qq}^{\theta 1}$ relatively minor, using \mathbf{Y}_{eq} instead of $\mathbf{Y}_{eq}^{\theta 1}$ may lead to similar stability assessment, while when the grid is weak, the interaction can no longer be ignored, $\mathbf{Y}_{eq}^{\theta 1}$ is necessary to be adopted to obtain a correct assessment. On the other hand, as shown in Fig. 7, a PLL with higher BW has a higher negative real part of the converter admittance. According to [21], this feature could further compromise the system stability.

By including the first-order $\Delta\theta'$ -related terms, the model can better reveal the dynamic behaviors introduced by the grid synchronization. In particular, when the PLL BW is high, or the grid is weak (i.e., $\text{SCR} < 3$), this impedance-based model can represent the most detailed phenomenon of a grid converter for static analysis, among the above-mentioned three models. Nevertheless, during transient analysis, using first-order Maclaurin expansion is inaccurate, which incurs error for system responses as well as stability analysis.

D. Impedance-Based With Higher-Order PLL Terms

During large phase perturbation, higher-order $\Delta\theta'$ -related terms of (17) have to be included in the model, which can better approximate the trigonometric functions during transient and therefore represent more accurate system responses. Take the second-order PLL terms as an example, the model can be rewritten by

$$\begin{aligned} \begin{bmatrix} \Delta i_d \\ \Delta i_q \end{bmatrix} &= \mathbf{I}_{eq} \begin{bmatrix} \Delta i_{dref} \\ \Delta i_{qref} \end{bmatrix} + \mathbf{Y}_{eq}^{\theta 1} \begin{bmatrix} \Delta v_d \\ \Delta v_q \end{bmatrix} + \begin{bmatrix} \Theta_{d2} \\ \Theta_{q2} \end{bmatrix} \Delta\theta'^2 \\ &= \mathbf{I}_{eq} \begin{bmatrix} \Delta i_{dref} \\ \Delta i_{qref} \end{bmatrix} + \mathbf{Y}_{eq}^{\theta 2} \begin{bmatrix} \Delta v_d \\ \Delta v_q \end{bmatrix} \end{aligned} \quad (23)$$

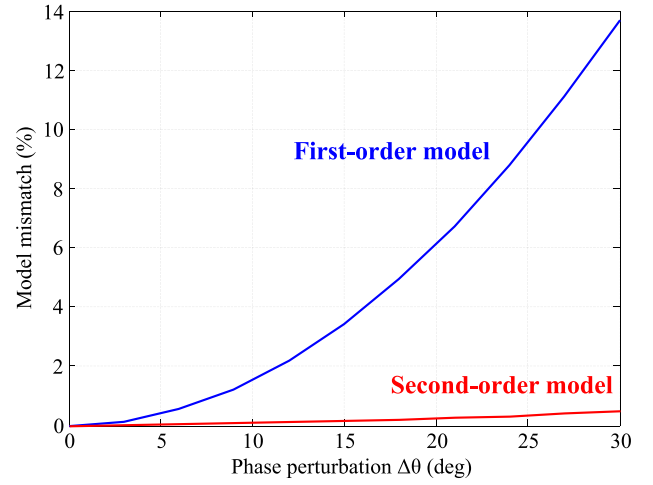


Fig. 8. Model evaluation during phase perturbations: model mismatches of first-order model (blue curve) and second-order model (red curve).

where

$$\begin{aligned} Y_{dd}^{\theta 2} &= Y_{dd}, Y_{qd}^{\theta 2} = Y_{qd}, \\ Y_{dq}^{\theta 2} &= Y_{dq}^{\theta 1} + 2\Delta\theta_p \Theta_{d2} G_{PLL_op}, \\ Y_{qq}^{\theta 2} &= Y_{qq}^{\theta 1} + 2\Delta\theta_p \Theta_{q2} G_{PLL_op}. \end{aligned} \quad (24)$$

Here, $\Delta\theta_p$ is the value of phase jump.

Comparisons of the accuracy and responses of (21) and (23) during phase perturbation is shown in Fig. 8. The mismatch percentages of the models with the first-order and the second-order PLL terms are given. The mismatch is calculated by the error between the simulation results and the model responses. It can be seen that the model with the first-order PLL terms has much higher mismatch (e.g., 10% mismatch higher when phase perturbation is $\pi/6$) than the model with the second-order terms. The mismatch of the second-order model is lower than 1% in the entire whole phase perturbation range. It is worth noting that the Maclaurin expansions with a higher-order for the trigonometric functions indeed provide a more accurate approximation, but higher computational efforts are required. Considering that $\pi/6$ is usually the upper limit in grid codes: the grid converter shall stay connection, the model with the second-order PLL is accurate enough for the analysis.

E. Modeling Scale Deepness and Accuracy Evaluation

The scale range for \mathbf{A} being the most accurate model respecting the converter behaviors during phase transient to \mathbf{E} being the least complicated model for power system analysis have been listed in Table II.

The scheduling and optimization of the power system represents the system steady-state view, which is employed for system design study or for simulation initialization study. The phenomenon of this problem involving fundamental frequency and sub-synchronous frequency, thus accurate model including the details of a grid converter is not necessary. Each converter

TABLE II
MODELING DEEPNESS AND ACCURACY EVALUATION FOR GRID CONVERTER

Accuracy	Problem	Grid condition	Modeling type
A	Transient stability	Weak grid with large phase perturbation	Impedance-based model with higher-order PLL terms
B	Harmonic stability using small-signal analysis	Weak grid ($SCR < 3$)	Impedance-based model with first-order PLL terms
C		Strong grid ($SCR > 10$)	Impedance-based model
D	Linear analysis	Strong grid ($SCR > 10$)	Current source model
E	Scheduling and optimization	Stiff grid	Phasorial model

can be represented as current/power injection in the connection bus by the phasorial model.

Linear analysis is important for the control design and stability of single grid converter component. This problem is mostly influenced by the current control and the plant, thus a current source model of (19) is enough for control performance evaluation in steady-state and stability assessment provided the grid converter being connected to a strong grid.

Small-signal analysis investigates on the responses of the system to small perturbations. This analysis allows to assess the harmonic stability caused by the control interactions and filter resonances. Therefore, the impedance model including the effects of various small-signal perturbations must be used. In case of the strong grid, the interaction between the grid impedance and the PLL can be ignored, only the effects of current and voltage perturbation shall be considered in the impedance-based model as (20). Nevertheless, if a weak grid is studied, the PLL dynamics could incur inter-area oscillation because of its interaction with the grid. Then, an impedance-based model with first-order PLL terms as (21) shall be used for the small-signal analysis and harmonic stability assessment.

Transient stability studies the capability of a system to remain stable after disturbances, in this paper the disturbance refer to the phase perturbation. For phase perturbation, PLL is required to achieve a satisfactory accuracy of the phenomena. Higher-order Maclaurin expansions are needed to better approximate the trigonometric functions related to the PLL and transform. Practically, the phase perturbation range for a grid converter is $\pi/6$ according to the grid codes. The impedance-based model with second-order PLL terms of (23) can achieve less than 1% model mismatch for the analysis.

V. SIMULATION AND EXPERIMENTAL RESULTS

In this section, different models presented in Section IV have been simulated and the limitation of each model under different scenarios are highlighted. The proposed impedance-based model with second-order PLL terms has been validated by experimental results and applied to a case study with stability concern, where different PLL BW are utilized.

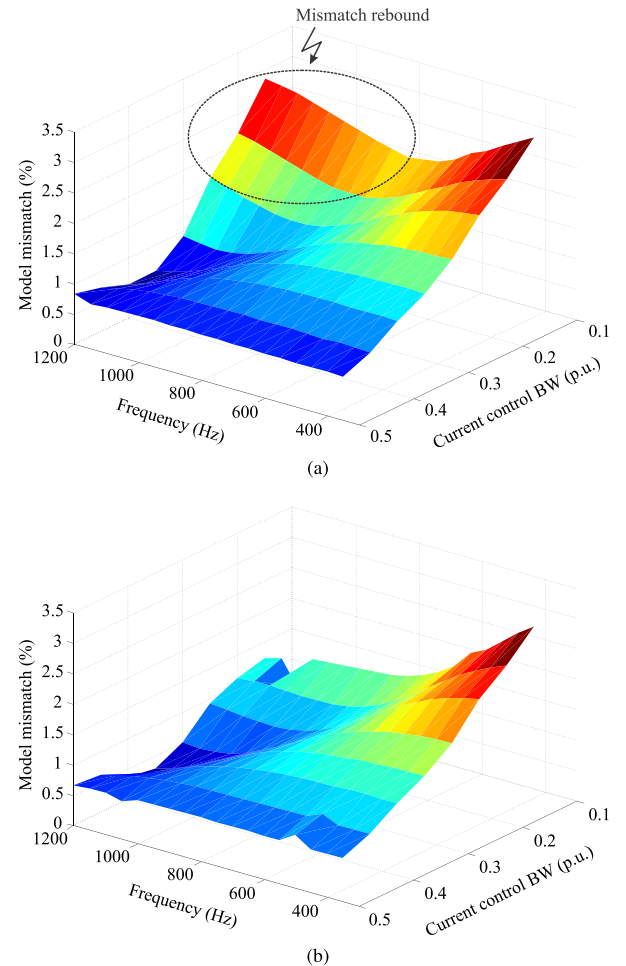


Fig. 9. Model mismatch in steady-state when using different models: (a) current source model and (b) impedance-based model.

A. Case Study

Firstly, the current source model and the impedance-based model without PLL are compared in terms of the steady-state accuracy. In this case study, current/voltage perturbations at

TABLE III
STABILITY BOUNDARY VERSUS PLL BANDWIDTH AND SCR

PLL BW \ SCR	60 Hz	80 Hz	100 Hz	120 Hz	140 Hz	160 Hz	180 Hz	200 Hz
1	Stable	Unstable	Unstable	Unstable	Unstable	Unstable	Unstable	Unstable
1.5	Stable	Stable	Unstable	Unstable	Unstable	Unstable	Unstable	Unstable
2	Stable	Stable	Stable	Stable	Stable	Unstable	Unstable	Unstable
2.5	Stable	Stable	Stable	Stable	Stable	Stable	Stable	Unstable
3	Stable	Stable	Stable	Stable	Stable	Stable	Stable	Stable

different frequencies are applied to the models and the mismatches between the model responses and the simulation results are presented in Fig. 9. The perturbation frequency is sweeping from 200 Hz to 1200 Hz with 50 Hz step. Different control bandwidth are studied, which varying from 0.1 to 0.5 Nyquist frequency. For the impedance-based model (shown in Fig. 9b), it can be seen that the values of mismatch within the frequency range are decreasing when the frequency increases. However, for the current source model (shown in Fig. 9a), the values of mismatch rebound when the frequency exceeds 1000 Hz, as being highlighted by the dashed circle as well as an arrow. The mismatch rebound is due to the ignorance of voltage perturbation for the current source model, as the effects of the voltage perturbation play an important role on the system response in that frequency range. On the other hand, the values of mismatch of both models are decreasing with the increasing of the control bandwidth, since a higher control bandwidth leads to higher contribution on system response. The accuracy of the current source model can approach the level of the impedance-based model when the bandwidth reaches 0.5 Nyquist frequency.

Secondly, the impedance-based model without PLL and the impedance-based model with first-order PLL terms are evaluated in terms of stability assessment during steady-state. For the impedance-based model with first-order PLL terms, the stability boundary versus the variation of PLL BW and grid SCR is shown in Table III, where the green region is the stable region, the red region indicates the system is unstable. It can be seen that the system stability is determined by both the PLL BW and the grid SCR. With the increasing of the BW or reducing the SCR, the system tends to be unstable during steady-state operation. However, if the impedance-based model without PLL is considered, all the cases in the table present stable condition. In this regard, the impedance-based model without PLL can achieve correct stability assessment regardless the grid representation up to 60 Hz PLL BW in this case study.

Thirdly, the impedance-based model with first- and second-order PLL terms are evaluated in terms of time-domain response and stability assessment during phase transient. The active/reactive power responses of a grid-interfaced converter are compared between simulation results and model responses under two scenarios, as shown in Fig. 10. In Fig. 10a, the grid converter operates at unity power factor, it can be seen that the responses of both the the impedance-based model with first- and second-order PLL terms can well match the simulation waveforms during steady state. However, when a phase jump

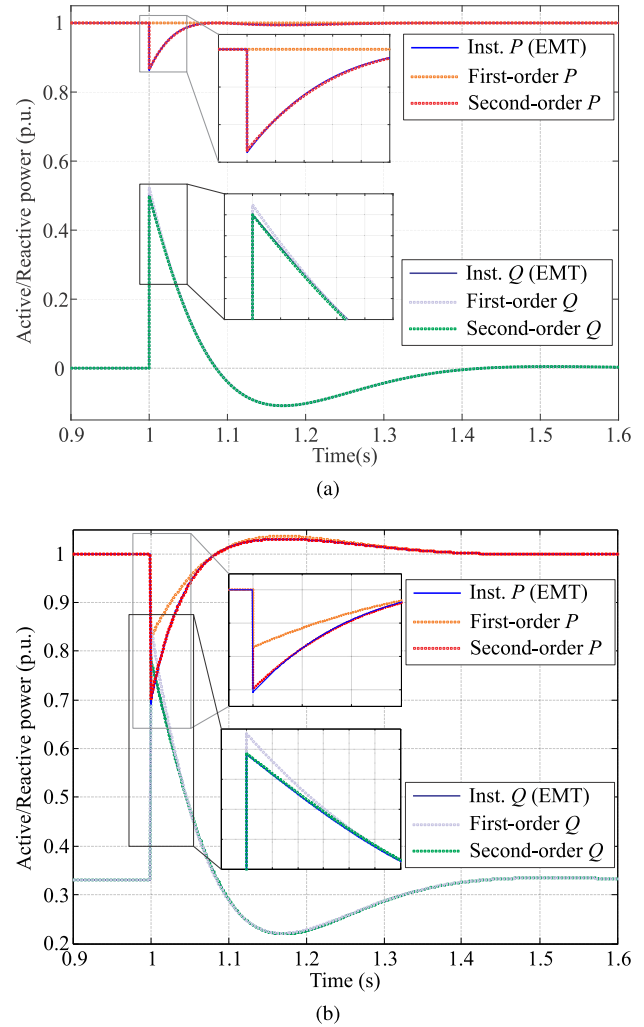
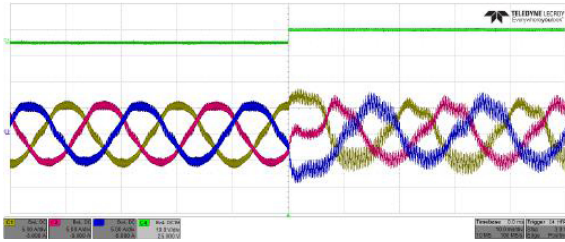


Fig. 10. Comparisons of active/reactive power between simulation results and PLL-based models under different scenarios: (a) unity power operation and (b) reactive compensation.

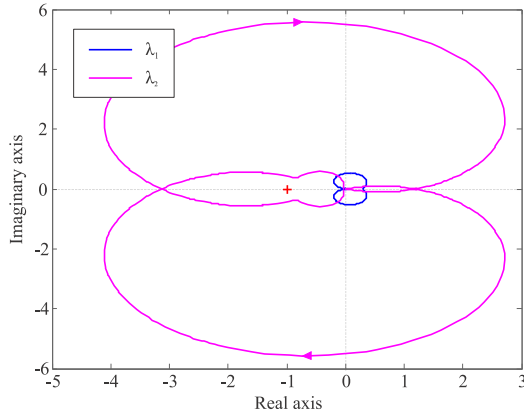
of $\pi/6$ occurs at $t = 1$ s, the responses of the first-order model can no longer follow the simulation waveforms, especially the active power response, leading to considerable model mismatch. On the other hand, the responses of the second-order model can well follow the simulation waveforms during transient stage. In Fig. 10b, the grid converter injects reactive power to grid, it can be seen that the model mismatch of the first-order model

TABLE IV
STABILITY BOUNDARY VERSUS PLL BANDWIDTH AND GRID PHASE PERTURBATION

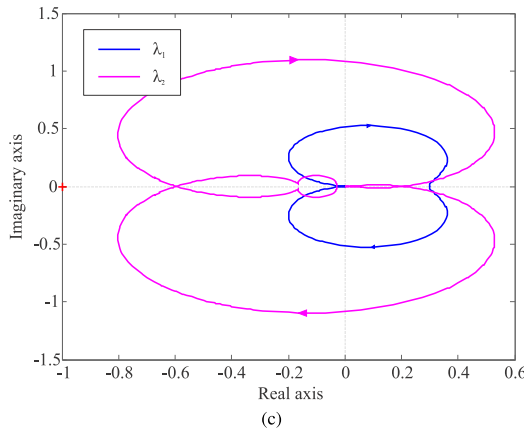
PLL BW \ Phase jump	180 Hz	182.5 Hz	185 Hz	187.5 Hz	190 Hz	192.5 Hz	195 Hz
5 deg ($\pi/36$)	Stable	Stable	Stable	Stable	Stable	Unstable	Unstable
10 deg ($\pi/18$)	Stable	Stable	Stable	Unstable	Unstable	Unstable	Unstable
15 deg ($\pi/12$)	Stable	Stable	Unstable	Unstable	Unstable	Unstable	Unstable
20 deg ($\pi/9$)	Stable	Stable	Unstable	Unstable	Unstable	Unstable	Unstable
25 deg ($5\pi/36$)	Stable	Stable	Unstable	Unstable	Unstable	Unstable	Unstable
30 deg ($\pi/6$)	Stable	Unstable	Unstable	Unstable	Unstable	Unstable	Unstable



(a)



(b)



(c)

Fig. 11. Stability assessment of a grid converter during phase jump of $\pi/6$: (a) experimental waveforms, (b) Nyquist diagrams of system characteristic loci using the impedance-based model with second-order PLL terms, and (c) Nyquist diagrams of system characteristic loci using the impedance-based model with first-order PLL terms.

is still significant, while the second-order model can maintain high accuracy during transient stage.

In addition, for the impedance-based model with second-order PLL terms, the stability boundary versus the variation of PLL BW and phase jump angle of grid voltage is shown in Table IV. It can be seen that the system stability is determined by both the PLL BW and the grid phase perturbation. With the increasing of the BW and phase jump angle, the system is less likely to be stable when a phase jump occurs. However, if the impedance-based model with first-order PLL terms is considered, all the cases in the table are stable according to the stability assessment. With this consideration, the impedance-based model with first-order PLL terms can well predict system stability up to $\pi/6$ phase jump when the PLL BW is lower than 180 Hz.

B. Experimental Validation

In order to validate the advantages of second-order model for transient analysis, in particular for the transient stability analysis, the system stability during phase transient is assessed by both the first-order and the second-order models. In this case study, the PLL BW of 200 Hz is used and the system becomes unstable after the phase jump of $\pi/6$ as shown in Fig. 11a. When the first-order model is used for the stability analysis, the Nyquist diagrams of the system characteristic loci are shown in Fig. 11c, where none of the system characteristic loci encircles the critical point indicating the system is stable but the fact is not. When the second-order model is used for the analysis, the Nyquist diagrams of the system characteristic loci are shown in Fig. 11b, where one system characteristic loci encircles the critical point indicating the system is unstable. As a result, the analysis using the second-order model can correctly assess the system stability during phase transient.

VI. CONCLUSION

Model of PLL-based synchronization in grid converters under normal grid condition has been developed in this paper. Comparing to the conventional models in the literature, the proposed model using full Maclaurin expansions can provide higher accuracy in power electronics and power systems analysis, especially for phase transient analysis. Moreover, the proposed model offers various representations, including phasorial model,

current source model, and impedance-based model without/with PLL effects. Each model representation uses certain term(s) of the proposed model, and it can reveal certain phenomenon though has limitation under certain circumstance. In this regard, a guideline on how to choose a proper model representation with sufficient accuracy has been proposed based on the grid conditions and problems to be studied. Simulation and experimental results have been given to verify the effectiveness of the model and analysis. Furthermore, the behaviors of PLL-based converter under unbalanced grid condition could be an interesting topic in future, where both the proposed Maclaurin expansions as well as double-frequency terms for the transform matrix would be considered in the modeling procedure.

APPENDIX

The detailed expressions of the matrix elements of \mathbf{I}_{eq} and \mathbf{Y}_{eq} are illustrated as followings:

$$Y_{dd} = Y_{qq} = \frac{(1 - G_d)(G_c G_d + L_f s)}{(G_c G_d + L_f s)^2 + L_f^2 \omega^2}$$

$$Y_{dq} = -Y_{qd} = \frac{(1 - G_d)L_f \omega}{(G_c G_d + L_f s)^2 + L_f^2 \omega^2} \quad (25)$$

$$I_{dd} = I_{qq} = \frac{G_c G_d (G_c G_d + L_f s)}{(G_c G_d + L_f s)^2 + L_f^2 \omega^2}$$

$$I_{dq} = -I_{qd} = \frac{G_c G_d L_f \omega}{(G_c G_d + L_f s)^2 + L_f^2 \omega^2} \quad (26)$$

where $G_f = L_f s$ is the transfer function of the output filter.

The detailed expressions of the matrix elements of PLL-related terms are

$$\Theta_{d1} = \frac{G_d(G_c + L_f s + L_f \omega)}{(G_c G_d + L_f s)^2 + L_f^2 \omega^2} \cdot (V_q - V_{rq}' - I_q G_c)$$

$$\Theta_{q1} = \frac{G_d(G_c + L_f s - L_f \omega)}{(G_c G_d + L_f s)^2 + L_f^2 \omega^2} \cdot (-V_d + V_{rd}' + I_d G_c)$$

$$\Theta_{d2} = \frac{G_d(G_c + L_f s + L_f \omega)}{(G_c G_d + L_f s)^2 + L_f^2 \omega^2} \cdot \left(-\frac{V_d}{2} - \frac{V_{rd}'}{2} - \frac{I_d}{2} G_c \right)$$

$$\Theta_{q2} = \frac{G_d(G_c + L_f s - L_f \omega)}{(G_c G_d + L_f s)^2 + L_f^2 \omega^2} \cdot \left(-\frac{V_q}{2} - \frac{V_{rq}'}{2} - \frac{I_q}{2} G_c \right). \quad (27)$$

The design criterion of PI parameters of SRF-PLL is given as follows. Based on (5), the closed-loop error transfer function can be obtained by

$$E_e(s) = \frac{k_{ppll}s + k_{ipll}}{s^2 + k_{ppll}s + k_{ipll}} \quad (28)$$

which is a second-order transfer function, and it can be written in a normalized way as

$$E_e(s) = \frac{2\xi\omega_n s + \omega_n^2}{s^2 + 2\xi\omega_n s + \omega_n^2} \quad (29)$$

where $\omega_n = \sqrt{k_{ipll}}$ and $\xi = \frac{k_{ppll}\sqrt{k_{ipll}}}{2k_{ipll}}$.

By using the approximated expression in [17], the settling time t_{sett} of a particular second-order system is

$$t_{sett} = 4.6\tau = \frac{4.6}{\xi\omega_n}. \quad (30)$$

Combining (30) with the normalized coefficients of (29), the PI parameter of SRF-PLL can be set as a function of settling time:

$$k_{ppll} = 2\xi\omega_n = \frac{9.2}{t_{sett}}$$

$$k_{ipll} = \omega_n^2 = \frac{4.6^2}{(t_{sett}\xi)^2} \quad (31)$$

To achieve an optimal damped second-order system, $\xi = \frac{1}{\sqrt{2}}$ is employed, and then the PI parameters can be obtained with given settling time. For instance, in Table I, the settling time was set to $t_{sett} = 500$ ms and the proportional and the integral gains of the PLL are 18.4 and 169.3, respectively.

REFERENCES

- [1] P. Rodriguez, J. Pou, J. Bergas, J. I. Candela, R. P. Burgos, and D. Boroyevich, "Decoupled double synchronous reference frame PLL for power converters control," *IEEE Trans. Power Electron.*, vol. 22, no. 2, pp. 584–592, Mar. 2007.
- [2] M. Karimi-Ghartemani, "Linear and pseudolinear enhanced phase-locked loop (EPLL) structures," *IEEE Trans. Ind. Electron.*, vol. 61, no. 3, pp. 1464–1474, Mar. 2014.
- [3] G. Buticchi, G. D. Carne, D. Barater, Z. Zou, and M. Liserre, "Analysis of the frequency-based control of a master/slave micro-grid," *IET Renewable Power Gener.*, vol. 10, no. 10, pp. 1570–1576, 2016.
- [4] Z. Zou, G. Buticchi, M. Liserre, A. M. Kettner, and M. Paolone, "Voltage stability analysis using a complete model of grid-connected voltage-source converters," in *Proc. IEEE Energy Convers. Congr. Expo.*, Sep. 2016, pp. 1–8.
- [5] R. Rosso, G. Buticchi, M. Liserre, Z. Zou, and S. Engelken, "Stability analysis of synchronization of parallel power converters," in *Proc. 43rd Annu. Conf. IEEE Ind. Electron. Soc.*, Oct. 2017, pp. 440–445.
- [6] W. Tang, F. C. Lee, and R. B. Ridley, "Small-signal modeling of average current-mode control," *IEEE Trans. Power Electron.*, vol. 8, no. 2, pp. 112–119, Apr. 1993.
- [7] J. Sun, "Small-signal methods for ac distributed power systems: A review," *IEEE Trans. Power Electron.*, vol. 24, no. 11, pp. 2545–2554, Nov. 2009.
- [8] L. Harnefors, M. Bongiorno, and S. Lundberg, "Input-admittance calculation and shaping for controlled voltage-source converters," *IEEE Trans. Ind. Electron.*, vol. 54, no. 6, pp. 3323–3334, Dec. 2007.
- [9] D. Dong, B. Wen, D. Boroyevich, P. Mattavelli, and Y. Xue, "Analysis of phase-locked loop low-frequency stability in three-phase grid-connected power converters considering impedance interactions," *IEEE Trans. Ind. Electron.*, vol. 62, no. 1, pp. 310–321, Jan. 2015.
- [10] M. Kazem Bakhshizadeh *et al.*, "Couplings in phase domain impedance modeling of grid-connected converters," *IEEE Trans. Power Electron.*, vol. 31, no. 10, pp. 6792–6796, Oct. 2016.
- [11] F. Blaabjerg, R. Teodorescu, M. Liserre, and A. V. Timbus, "Overview of control and grid synchronization for distributed power generation systems," *IEEE Trans. Ind. Electron.*, vol. 53, no. 5, pp. 1398–1409, Oct. 2006.
- [12] S. Golestan, M. Monfared, F. D. Freijedo, and J. M. Guerrero, "Design and tuning of a modified power-based PLL for single-phase grid-connected power conditioning systems," *IEEE Trans. Power Electron.*, vol. 27, no. 8, pp. 3639–3650, Aug. 2012.
- [13] P. Rodriguez, J. Pou, J. Bergas, J. I. Candela, R. P. Burgos, and D. Boroyevich, "Decoupled double synchronous reference frame PLL for power converters control," *IEEE Trans. Power Electron.*, vol. 22, no. 2, pp. 584–592, Mar. 2007.
- [14] M. L. Boas, *Mathematical Methods in the Physical Sciences*. New York, NJ, USA: Wiley, 2006.
- [15] E. On-Netz, *Grid Code. High and Extra High Voltage*, E.ON Netz GmbH, Bayreuth Std., Bayreuth, Germany, Apr. 2009.

- [16] Energinet, *Technical Regulation 3.2.5 for Wind Power Plants With a Power Output Greater Than 11 kW*. Fredericia, Denmark: Energinet, 2010.
- [17] G. Franklin, J. Powell, and A. Emami-Naeini, *Feedback Control of Dynamic Systems*, 4th ed. Englewood Cliffs, NJ, USA: Prentice-Hall, 2002.
- [18] X. Wang, F. Blaabjerg, and W. Wu, "Modeling and analysis of harmonic stability in an ac power-electronics-based power system," *IEEE Trans. Power Electron.*, vol. 29, no. 12, pp. 6421–6432, Dec. 2014.
- [19] X. Wang and F. Blaabjerg, "Harmonic stability in power electronic-based power systems: Concept, modeling, and analysis," *IEEE Trans. Smart Grid*, vol. 10, no. 3, pp. 2858–2870, May 2019.
- [20] N. P. W. Strachan and D. Jovic, "Stability of a variable-speed permanent magnet wind generator with weak ac grids," *IEEE Trans. Power Del.*, vol. 25, no. 4, pp. 2779–2788, Oct. 2010.
- [21] B. Wen, D. Boroyevich, R. Burgos, P. Mattavelli, and Z. Shen, "Analysis of d-q small-signal impedance of grid-tied inverters," *IEEE Trans. Power Electron.*, vol. 31, no. 1, pp. 675–687, Jan. 2016.



Zhi-Xiang Zou (S'12–M'18) received the B.Eng. and Ph.D. degrees in electrical engineering from Southeast University, Nanjing, China, in 2007 and 2014, respectively.

From 2007 to 2009, he was an Engineer with the State Grid Electric Power Research Institute, Nanjing, China. He is currently a Scientific Staff Member with the Chair of Power Electronics, University of Kiel, Kiel, Germany. His research interests include smart transformers, microgrid stability, and control of grid converters.

Dr. Zou is currently an Associate Editor for the *IEEE ACCESS*, an Editor for the *International Transactions on Electrical Energy Systems*, and the *Mathematical Problem in Engineering*.



Marco Liserre (S'00–M'02–SM'07–F'13) received the M.Sc. and Ph.D. degrees in electrical engineering from Bari Polytechnic, Bari, Italy, in 1998 and 2002, respectively.

He has been an Associate Professor with Bari Polytechnic, and, since 2012, a Professor in reliable power electronics with Aalborg University, Aalborg, Denmark. Since 2013, he has been a Full Professor, and he holds the Chair of Power Electronics with the Kiel University, Kiel, Germany, where he leads a team of more than 20 researchers with an annual budget of two million Euro and cooperation with 20 companies. He has authored or coauthored more than 350 technical papers (more than 110 of them in international peer-reviewed journals) and a book.

Dr. Liserre's works have received more than 25 000 citations. He is listed in the ISI Thomson report "The world's most influential scientific minds" from 2014. He has been awarded with an ERC Consolidator Grant for the project "The Highly Efficient And Reliable smart Transformer (HEART), a New Heart for the Electric Distribution System" and with the ERC Proof of Concept Grant U-HEART. He is a member of Industry Application Society (IAS), Power Electronics Society (PELS), Power and Energy Society (PES), and Industrial Electronics Society (IES). He has been serving all these societies in different capacities. He was the recipient of the IES 2009 Early Career Award, the IES 2011 Anthony J. Hornfeck Service Award, the 2014 Dr. Bimal Bose Energy Systems Award, the 2011 Industrial Electronics Magazine Best Paper Award the Third Prize Paper Award by the Industrial Power Converter Committee at IEEE Energy Conversion Congress and Exposition 2012, the 2017 IEEE PELS Sustainable Energy Systems Technical Achievement Award, and the 2018 IEEE IES Mittelmann Achievement Award, which is the highest award of the IEEE-IES.